



HAL
open science

Decomposition of the CO stretching vibration band of laboratory H₂O-CO ices irradiated by heavy ions

E Seperuelo Seperuelo Duarte, A L F de Barros, E F da Silveira, Alicja Domaracka, P Boduch, H Rothard

► **To cite this version:**

E Seperuelo Seperuelo Duarte, A L F de Barros, E F da Silveira, Alicja Domaracka, P Boduch, et al.. Decomposition of the CO stretching vibration band of laboratory H₂O-CO ices irradiated by heavy ions. Monthly Notices of the Royal Astronomical Society, 2021, 10.1093/mnras/stab2806 . hal-03426597

HAL Id: hal-03426597

<https://hal.science/hal-03426597v1>

Submitted on 12 Nov 2021

HAL is a multi-disciplinary open access archive for the deposit and dissemination of scientific research documents, whether they are published or not. The documents may come from teaching and research institutions in France or abroad, or from public or private research centers.

L'archive ouverte pluridisciplinaire **HAL**, est destinée au dépôt et à la diffusion de documents scientifiques de niveau recherche, publiés ou non, émanant des établissements d'enseignement et de recherche français ou étrangers, des laboratoires publics ou privés.

Decomposition of the CO stretching vibration band of laboratory H₂O-CO ices irradiated by heavy ions

E. Seperuelo Duarte¹, A. L. F. de Barros², E. F. da Silveira³, A. Domaracka⁴, P. Boduch⁴, H. Rothard⁴

¹ Instituto Federal de Educação, Ciência e Tecnologia, Rio de Janeiro, RJ, Brazil.

² Departamento de Física, Centro Federal de Educação Tecnológica Celso Suckow da Fonseca, Av. Maracanã 229, 20271-110 Rio de Janeiro, RJ, Brazil.

³ Departamento de Física, Pontifícia Universidade Católica do Rio de Janeiro, Rua Marquês de São Vicente 225, 22451-900, Rio de Janeiro, RJ, Brazil.

⁴ Centre de Recherche sur les Ions, les Matériaux et la Photonique (CEA/CNRS/ENSICAEN/UNICAEN/Normandie Univ.), CIMAP-CIRIL-Ganil

Received

ABSTRACT

H₂O and CO molecules are the main constituents of the interstellar dust grain ice mantles. Infrared spectra of the ices in line of sights of young stellar objects and background stars have shown that the CO stretching vibration band can be decomposed into three main components: 2143, 2139 and 2136 cm⁻¹, assigned to CO in different environment sites. The relative strengths between the components have been associated to an evolutionary track of the interstellar molecular clouds. H₂O:CO (3:2) and (10:1) ices samples were irradiated by 0.79 MeV/u ⁵⁸Ni¹³⁺ ions to simulate the effects produced by heavy ion cosmic rays in typical interstellar ices mixtures. The CO stretching vibration band is decomposed into six Gaussians functions (2150, 2144, 2141, 2138, 2136 and 2133 cm⁻¹) and their integrated absorbances were measured as a function of fluence. The results have shown that, at the final fluence, the component 2138 cm⁻¹ is the main component of the CO stretching vibration band. The component 2150 cm⁻¹ disappears at the beginning of irradiation. Based on the present and previous results, a time scale for the components in the interstellar ices is proposed. For H₂O:CO ice in the ISM it is predicted that, after 1 Myrs, the main components of the CO stretching vibration band are the 2138 cm⁻¹ and 2141 cm⁻¹, due to the CO monomers and dimers, respectively.

Key words: astrochemistry – methods: laboratory – ISM: Ice mantles

1 INTRODUCTION

It is well accepted that H₂O and CO molecules are the main molecular constituents of interstellar cloud ices. Based on infrared spectroscopic observations, two molecular structures have been proposed for describing H₂O:CO ice mixtures: (i) ice layers with the molecules segregated or (ii) ice with the molecules homogeneously mixed (Pontoppidan et al. 2003). In the first one, the condensed water molecules are believed to be produced on grain surfaces by chemical reactions on grain surfaces containing hydrogen atoms, oxygen atoms and OH radicals (Tielens & Hagen 1982; Boogert & Ehrenfreund 2004; Ioppolo et al. 2008). This first layer, composed mainly by water molecules, would be produced in the early stages of the cloud. As the molecular clouds evolve, the CO molecules, which are relatively abundant in the gas phase, condense on dust grains capped by water ices (Aikawa et al. 2001; Pontoppidan et al. 2003). For the second molecular configuration, the CO molecules would condense on grains concomitantly with water molecule formation, generating H₂O:CO ice mixtures. The latter could also be formed in the first scenario if the layers were processed either by grain temperature increase or by cosmic ray irradiation (Collings et al. 2003).

Laboratory experiments have shown that the infrared CO stretching vibration band at ~ 2138 cm⁻¹ is highly affected by the environment. When CO is co-deposited with H₂O, this band widens and shifts towards lower frequencies. In addition, a new band feature arises at ~ 2150 cm⁻¹. The primary band may be described by two Gaussians: 2139 and 2136 cm⁻¹. Al-Halabi et al. (2004) assigned those vibrations to different sites of interactions for CO molecules. The 2150 cm⁻¹ feature is associated with the interaction between CO and OH dangling bond. The 2139 cm⁻¹ band has two assignments: (i) CO interacting with another CO molecule (or any other apolar molecule) and (ii) CO interacting with an OH bonded with another water molecule (it is important to note that this component is associated with CO on the ice surface similarly to that associated with 2150 cm⁻¹). The 2136 cm⁻¹ component is associated with a CO substituting a water molecule in the matrix.

Pontoppidan et al. (2003) observed the interstellar medium (ISM) towards different lines of sight. They showed that the CO band profiles are constituted by three components at: 2143.7, 2139.9 and 2136.5 cm⁻¹. The blue (short-wavelength) component at 2143.7 cm⁻¹ is associated with the CO crystalline ice when the background source is linearly polarized (longitudinal optical (LO) component). However, this band is also associated with the CO interaction with other molecules such as CO₂, O₂ and N₂ (Boogert et al. 2002). Pontoppidan et al. (2003) have associated the 2139 cm⁻¹ component with pure CO ice layers on top of water ices. However, the observation of the 2136 cm⁻¹ component is an evidence of CO trapped in the H₂O matrix. The 2150 cm⁻¹ component is not observed in the ISM, suggesting a presence of a compact

ice structure. In laboratory, the CO - OH db is rapidly destroyed by UV and ion irradiations (Al-Halabi et al. 2004). The lack of this band in interstellar medium is considered an evidence of the ice processing.

In the current work, H₂O:CO ice mixtures, prepared in a pre-chamber in two different concentrations (1:1 and 10:1) and deposited onto a cold (15 K) CsI substrate, were irradiated by 46 MeV ⁵⁸Ni¹¹⁺ ions and analyzed by Fourier Transform Infrared Spectroscopy (FTIR). Ni ions are present in cosmic rays and their physico-chemical effects are representative of all heavy ("metallic") constituents of cosmic rays, such as Fe, S and Mg. These effects follow known scaling laws as a function of electronic energy stopping power. The same behavior is also observed for the more abundant H⁺ or He⁺ ions (see, e.g. (Rothard et al. 2017; Dartois et al. 2013, 2015; Duarte et al. 2009, 2010; de Barros et al. 2011a, 2012; Mejía et al. 2015; Pereira et al. 2020)).

The CO stretching vibration band is decomposed into six Gaussian functions. In section 2, the ice preparation and the CO decomposition process are described. In section 3, the results of decompositions as a function of irradiation fluence are discussed and associated to the ice binding sites. In Section 4, the astrochemical implications are discussed and in section 5 the major findings are summarized.

2 EXPERIMENTAL

2.1 Ice preparation

MeV heavy ion beams delivered by the GANIL facility (Caen, France) allow mimicking the effects of cosmic ray bombardment on icy surfaces. After acceleration, the projectiles were directed into the CASIMIR set-up mounted on the IRRSUD beamline. The ice temperature was kept at 15 K by a closed-cycle helium cryostat during the ice deposition and irradiation. The experimental apparatus is described elsewhere (Duarte et al. 2009, 2010; de Barros et al. 2011a,b).

Two different ice layers were deposited and sequentially irradiated. A gas mixing chamber was used and connected to the vacuum chamber. The H₂O vapor at 15 mbar was mixed with CO gas in an adequate partial pressure and then injected via a thin tube onto the cold CsI IR transparent window at 15 K. For the water target, an ultra pure liquid water with an electric conductivity of 10⁷ Ω cm (Milli-Q) was used; for the CO, the purity of the gas was 99.995% (Messer Griesheim). Once the target was prepared, a thin ice layer deposited on a CsI substrate is placed in the center of the vacuum chamber and under a residual gas pressure of 2 × 10⁻⁸ mbar at 15 K and irradiated by 46 MeV ⁵⁸Ni¹³⁺ ions up to a final fluence of ~ 5.3 × 10¹³ ions.cm⁻² and 1 × 10¹³ ions.cm⁻², respectively. The flux was maintained at 1 × 10⁹ ions.cm⁻².s⁻¹ in both cases. The samples were analyzed in situ by FTIR spectroscopy.

The range of the projectiles in H₂O:CO ice calculated, by the SRIM code Ziegler et al. (2010), is 24 μm. Thus, the projectiles traverse the thin layers with approximately constant velocity and interact with the sample molecules with the same cross section. At 46 MeV, the projectile electronic stopping power is much greater than the nuclear stopping power. Two different ice layers were deposited and sequentially irradiated. In Table 3, the total initial column density (N₀ⁱ = N₀(H₂O) + N₀(CO)), ice thicknesses, ion total fluence and electronic and nuclear stopping powers are shown for each concentration. The ice films infrared (IR) spectra (5000 - 600 cm⁻¹) were obtained with a spectral resolution of 1 cm⁻¹ using a Nicolet FTIR spectrometer (Magna 550). Figure 1 shows the IR spectra for both H₂O:CO ice mixture concentrations, before and after the irradiation. Since the intense stretch H₂O vibration band at 3280 cm⁻¹ is saturated for the ice mixture (10:1), the water column density was thus determined by using the 760 cm⁻¹ band absorbance. It is important to note that, a smallest feature at 2342 cm⁻¹ is attributed to CO₂ appear at non irradiated spectrum, probably condensed from the residual gas in the vacuum chamber. However, its abundance in the ices is about 0.03%.

2.2 CO decomposition

The infrared profile of the CO after the co-deposition of the gas mixture of H₂O and CO at 15 K shows two main features at 2138.3 and 2148.7 cm⁻¹ (1:1 concentration) and at 2136.2 and 2151.7 cm⁻¹ (10:1 concentration). In general, the irradiation narrows the main feature and destroy the component around 2150 cm⁻¹. Many small structures rise on the main feature wings suggesting the existence of different CO binding sites. The fitting approach adopted here was to find the smaller number of components that could describe all of the CO profiles of the infrared spectra of the irradiated ices. The CO profile of the (3:2) ice irradiated by 5 × 10¹¹ ions.cm⁻² was used as the starting point since the narrowing of the main component allowed us to identify the smaller components (Figure 2). A set of gaussians were used to determine the component positions and FWHM. This first component set was used to fit the other infrared spectra of the ice irradiated with different fluence values. Then, the positions and FWHM were averaged and the fitting procedure was repeated for the whole set of CO profiles. After many trials and errors, it is seen that all CO profiles can be fitted by six gaussian components with the positions and FWHM shown in Tables 1 and 2. In general, the fits are excellent as can be seen from the reduced χ² values in Tables 1 and 2 by visual inspection (Figures 3 and 4). The identifications and assignments of these components are discussed in Section 3.

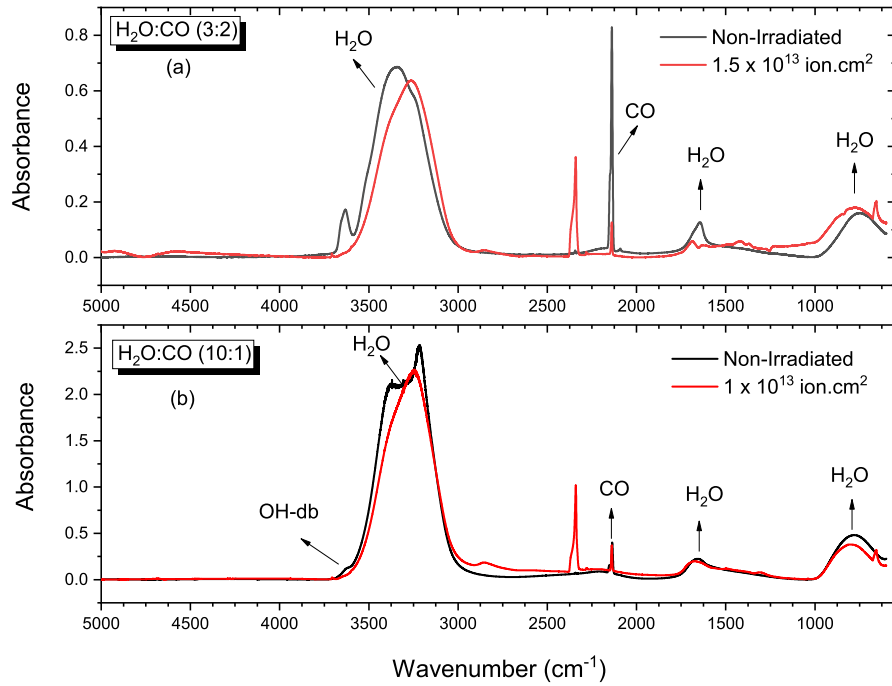


Figure 1. Mid-IR spectra of the H₂O:CO ice at 15 K for: (a) the non-irradiated sample and at 1.5×10^{13} fluence for the (3:2) mixture; and (b) for the non-irradiated and at 1.0×10^{13} fluence for the (10:1) mixture.

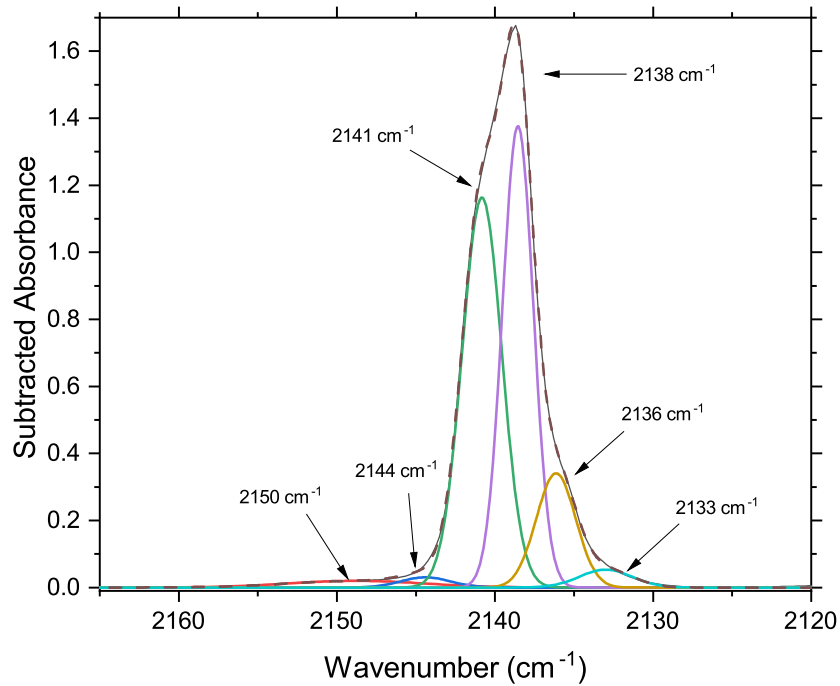


Figure 2. CO stretching vibration band of the (3:2) ice concentration irradiated by 1×10^{11} ions cm⁻². Six Gaussian functions are used to fit the whole wavenumber region. The subtracted absorbance means that the total absorbance has been subtracted by a background continuum.

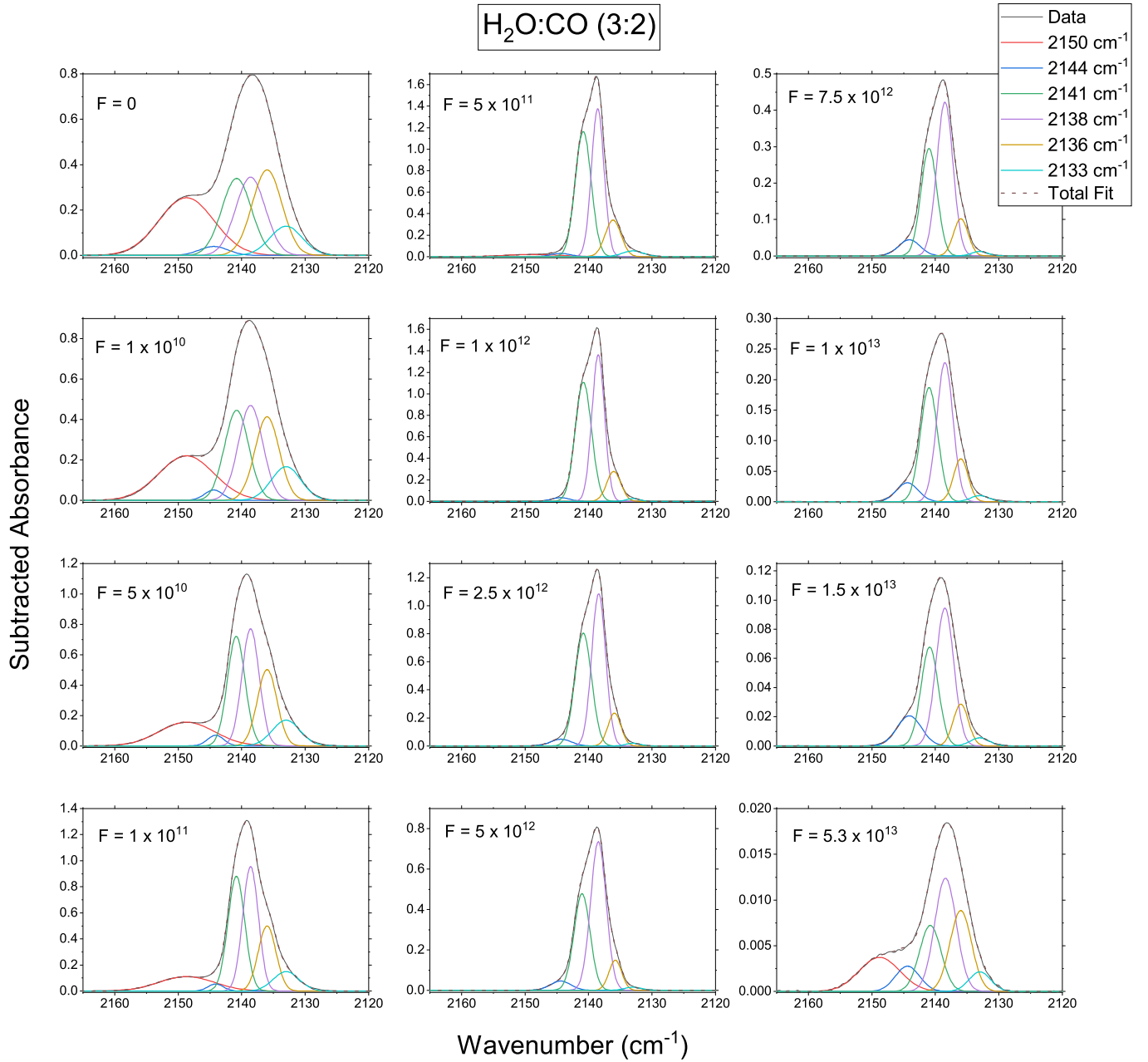


Figure 3. Decomposition of the CO stretching vibration band of the (3:2) ice concentration as a function of fluence. The fluence values in the panels are given in ions.cm⁻². Data of the last irradiation at 5.3×10^{13} ions.cm⁻² were not used in the fittings analysis.

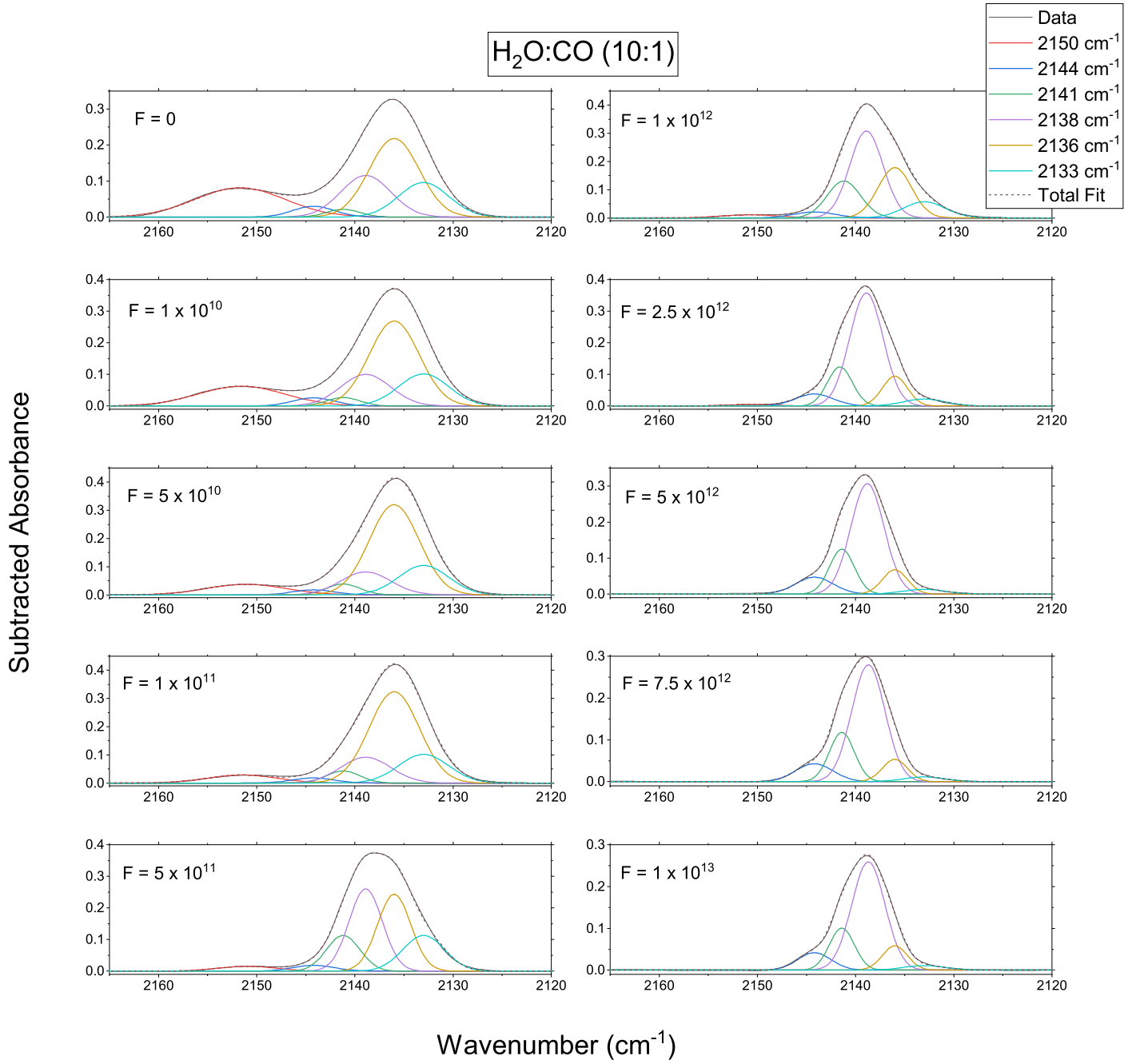


Figure 4. Decomposition of the CO stretching vibration band of the (10:1) ice concentration as a function of fluence. The fluence values in the panels are given in ions.cm⁻².

Table 1. Deconvolution of bands of CO as a function of fluence in 10^{10} ions.cm $^{-2}$.

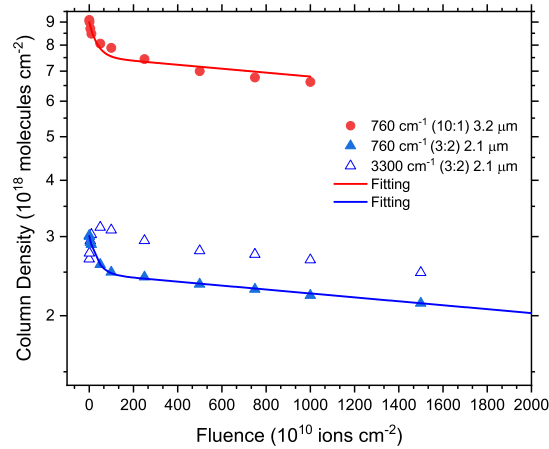
Fluence	(3:2) ice concentration															χ^2 (10 $^{-6}$)			
	2150 cm $^{-1}$			2144 cm $^{-1}$			2141 cm $^{-1}$			2138 cm $^{-1}$			2136 cm $^{-1}$				2133 cm $^{-1}$		
	W (cm $^{-1}$)	IA (cm $^{-1}$)	FWHM (cm $^{-1}$)	W (cm $^{-1}$)	IA (cm $^{-1}$)	FWHM (cm $^{-1}$)	W (cm $^{-1}$)	IA (cm $^{-1}$)	FWHM (cm $^{-1}$)	W (cm $^{-1}$)	IA (cm $^{-1}$)	FWHM (cm $^{-1}$)	W (cm $^{-1}$)	IA (cm $^{-1}$)	FWHM (cm $^{-1}$)		W (cm $^{-1}$)	IA (cm $^{-1}$)	FWHM (cm $^{-1}$)
0	2148.7	2.76	10.2	2144.4	0.225	5.35	2140.8	1.99	5.50	2138.6	2.02	5.50	2136.0	2.21	5.50	2133.0	0.823	6.00	4.7
1	2148.7	2.39	10.2	2144.4	0.186	3.40	2140.8	2.14	4.50	2138.6	2.25	4.50	2136.0	1.98	4.50	2133.0	0.976	5.50	5.6
5	2148.7	1.69	10.2	2144.1	0.224	3.00	2140.9	2.51	3.27	2138.6	2.63	3.21	2136.0	1.93	3.62	2133.0	0.921	5.12	10
10	2148.7	1.22	10.3	2144.1	0.164	2.83	2140.8	2.92	3.12	2138.6	2.94	2.90	2136.0	1.75	3.28	2133.0	0.763	4.79	15
50	2148.8	0.216	10.2	2144.4	0.120	3.70	2140.8	3.66	2.96	2138.6	3.38	2.31	2136.1	1.06	2.93	2133.0	0.222	3.92	27
100				2144.4	0.121	3.36	2140.8	3.53	3.00	2138.5	3.37	2.33	2136.0	0.776	2.62	2133.0	0.0666	2.39	30
250				2144.4	0.200	3.90	2140.8	2.63	3.08	2138.4	2.98	2.58	2135.9	0.600	2.41	2133.0	0.0559	2.67	9.1
500				2144.4	0.188	3.81	2141.0	1.52	2.98	2138.5	2.25	2.88	2135.8	0.375	2.36	2133.0	0.0528	3.16	2.9
750				2144.1	0.188	4.00	2141.0	0.942	3.00	2138.5	1.35	3.00	2136.0	0.293	2.70	2133.0	0.0394	3.00	3.5
1000				2144.4	0.133	4.00	2141.0	0.637	3.20	2138.5	0.727	3.00	2136.0	0.202	2.70	2133.0	0.0375	3.50	0.85
1500				2144.1	0.0989	4.50	2140.9	0.231	3.20	2138.5	0.332	3.30	2136.0	0.0853	2.80	2133.0	0.0207	3.50	0.22
5300	2148.8	0.0298	7.50	2144.4	0.0132	4.50	2140.8	0.0308	4.00	2138.4	0.0527	4.00	2136.0	0.0377	4.00	2133.0	0.00914	4.00	0.0089

Table 2. Deconvolution of bands of CO as a function of fluence in 10¹⁰ ions.cm⁻².

Fluence (cm ⁻¹)	(10:1) ice concentration												χ^2 (10 ⁻⁶)						
	2150 cm ⁻¹			2144 cm ⁻¹			2141 cm ⁻¹			2138 cm ⁻¹				2136 cm ⁻¹			2133 cm ⁻¹		
	W (cm ⁻¹)	IA (cm ⁻¹)	FWHM (cm ⁻¹)	W (cm ⁻¹)	IA (cm ⁻¹)	FWHM (cm ⁻¹)	W (cm ⁻¹)	IA (cm ⁻¹)	FWHM (cm ⁻¹)	W (cm ⁻¹)	IA (cm ⁻¹)	FWHM (cm ⁻¹)		W (cm ⁻¹)	IA (cm ⁻¹)	FWHM (cm ⁻¹)	W (cm ⁻¹)	IA (cm ⁻¹)	FWHM (cm ⁻¹)
0	2151.7	0.937	10.8	2144.2	0.160	5.00	2141.2	0.0915	4.00	2138.9	0.738	6.00	2136.0	1.39	6.00	2133.0	0.613	6.00	1.8
1	2151.6	0.697	10.4	2144.2	0.138	5.00	2141.2	0.115	4.00	2138.9	0.639	6.00	2136.0	1.72	6.00	2133.0	0.649	6.00	1.5
5	2151.1	0.380	9.48	2144.2	0.0946	5.00	2141.2	0.164	4.00	2138.9	0.520	6.00	2136.0	2.04	6.00	2133.0	0.667	6.00	2.3
10	2151.5	0.255	8.37	2144.2	0.0961	5.00	2141.2	0.182	4.00	2138.9	0.583	6.00	2136.0	2.07	6.00	2133.0	0.649	6.00	4.3
50	2151	0.114	6.93	2144.2	0.0982	5.00	2141.2	0.481	4.00	2138.9	1.11	4.00	2136.0	1.03	4.00	2133.0	0.602	5.00	3.0
100	2150.7	0.0777	6.69	2144.2	0.112	5.00	2141.2	0.557	4.00	2138.9	1.31	4.00	2136.0	0.759	4.00	2133.0	0.304	5.00	3.3
250	2150.7	0.0301	5.92	2144.2	0.183	4.50	2141.6	0.394	3.00	2138.9	1.52	4.00	2136.0	0.301	3.00	2133.0	0.118	5.00	2.1
500				2144.2	0.225	4.50	2141.4	0.397	3.00	2138.8	1.31	4.00	2136.0	0.215	3.00	2133.0	0.0703	5.00	1.5
750				2144.2	0.205	4.50	2141.4	0.376	3.00	2138.7	1.19	4.00	2136.0	0.170	3.00	2133.0	0.0602	5.00	1.4
1000				2144.2	0.177	4.00	2141.4	0.321	3.00	2138.7	1.10	4.00	2136.0	0.186	3.00	2133.0	0.0584	5.00	1.6

Table 3. H₂O:CO ice physical parameters: molecular concentration, the total initial column density ($N'_0 = N_0(\text{H}_2\text{O}) + N_0(\text{CO})$) and the ice thickness. Irradiation parameters: total ion fluence, electronic stopping power (S_e) and nuclear stopping power (S_n).

Concentration	N'_0 (molecules cm^{-2})	Thickness (μm)	Total fluence (10^{13} ions. cm^{-2})	S_e (10^3 keV. μm^{-1})	S_n (keV. μm^{-1})
(3:2)	4.7	2.1	5.3	3.6	11.7
(10:1)	10	3.4	1.0	3.6	11.7

**Figure 5.** H₂O column densities as a function of fluence measured by the 3300 cm^{-1} and 760 cm^{-1} bands. The 3300 cm^{-1} band of the (10:1) ice is saturated (see Fig. 1). Thus, for this ice concentration, the H₂O column density was determined by the 760 cm^{-1} band. The column density of the 760 cm^{-1} band were fitted by the sum of two exponential functions (solid lines): $N = N_1 \exp(-\sigma_1 F) + N_2 \exp(-\sigma_2 F)$. The cross sections are presented in Table 4. The column densities are supposed to be straight lines in semi-log scale; this does not occur because compaction affects the A-values.

3 RESULTS

3.1 H₂O column density

For the (3:2) mixture, the water column density was determined by the 3300 and 760 cm^{-1} bands; the measured absorbances correspond to 2.7×10^{18} molecules cm^{-2} and 3.0×10^{18} molecules cm^{-2} , respectively. They agree with each other within 10%. For the (10:1) mixture, the stretching mode absorbance at 3300 cm^{-1} band had saturated; thus, the water column density was calculated via the 760 cm^{-1} band. Column densities are expected to decrease exponentially with fluence and do not depend on the selected band according to the Lambert-Beer law. However, compaction alters the A-value of each band and – if this correction is not taken into account – column densities appear as a sum of two exponential; moreover, for the same concentration, they do not coincide for different bands. This is illustrated in Figure 5, which shows the water column densities as a function of fluence (F). Under these conditions, the column densities (N) obtained for the 760 cm^{-1} band are fitted by the sum of two exponential functions (Eq.(1)). See details in Mejía et al. (2015).

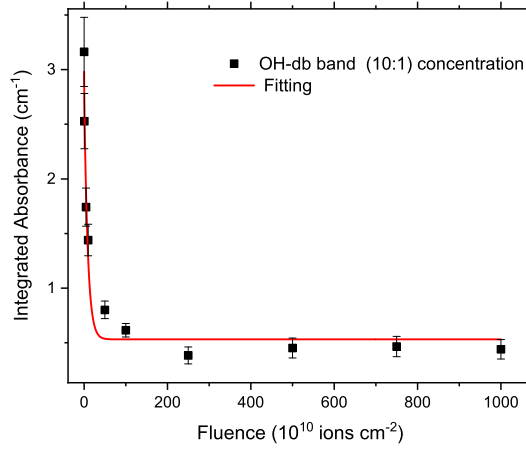
$$N = N_1 \exp(-\sigma_1 F) + N_2 \exp(-\sigma_2 F) \quad (1)$$

where N_1 and N_2 are constants and σ_1 and σ_2 are the compaction and destruction cross sections, respectively. Nevertheless, the same compaction cross section is extracted for the two measurements (see Table 4). This result shows that the H₂O 760 cm^{-1} cross sections are not affected by the thickness difference between the ices.

The compaction cross section can also be obtained by the OH dangling bond in the 3700 - 3560 cm^{-1} range. In both concentrations, the OH-db integrated absorbance decrease very fast at the beginning of irradiation ($F < 5 \times 10^{11}$ ions. cm^{-2}). However, it does not go to zero possibly due to a deposition of a new water layer from the residual gas. The data were fitted by one exponential law and the cross sections found were 1.1×10^{-11} cm^2 (3:2) and 1.2×10^{-11} cm^2 (10:1) as shown in Fig. 6. Although the discrepancy with the results found by the 760 cm^{-1} bend mode, they are consistent with the power law found by Dartois et al. (2013) (Figure 3) in which the OH dangling bond cross section scale with the electronic stopping power ($\sigma \sim S_e^1$). For the electronic stopping power of the current work, the cross sections values found here are within the boundaries of the power law uncertainties.

Table 4. The cross sections (in 10^{-13} cm²) and column densities (in 10^{18} molecules cm⁻²) of the H₂O and CO main features.

	(3:2)				(10:1)			
	σ_1	σ_2	N_1	N_2	σ_1	σ_2	N_1	N_2
H ₂ O bend mode 760 cm ⁻¹	27	0.1	0.53	2.5	27	0.1	1.5	7.5
CO Total	41	1.6	0.14	2.0	9.2	0.35	0.30	0.55


Figure 6. OH-db integrated absorbance (10:1) as a function of fluence and corresponding fitted exponential law. The cross section obtained by the fitting is 1.2×10^{-11} cm².

3.2 CO stretching vibration components

The CO stretching vibration profile shows a set of complex components variation as a function of fluence and in this section the identifications are discussed.

As seen in the previous section, all CO stretching bands are fit by the sum of 6 gaussians in both ice mixture concentrations. The averaged positions of these components changes from one concentration to another, but all of them can be assigned to the same respective CO binding sites.

The 2150 cm⁻¹ component:

The component at about 2150 cm⁻¹ appears on the infrared spectrum when CO is mixed with water. It is well established that this feature is associated to the CO stretching vibration when the molecule interacts with the OH dangling bonds. Before irradiation, the component is centered on 2148.7 cm⁻¹ with FWHM of 10.2 cm⁻¹ in the (3:2) ice concentration and shifts toward the blue at 2151.7 cm⁻¹ with FWHM of 10.8 cm⁻¹ in the (10:1) concentration. Spectroscopy identification of CO - H₂O clusters trapped in argon matrix has shown that in this region the infrared features are associated to clusters formed by CO molecules and H₂O molecules (Abe & Yamada 2001) (Abe & Yamada 2004). The smallest cluster (H₂O - CO) produces an absorption at 2149.4 cm⁻¹ and shifts toward the red (longer wavelength) component as the number of CO molecules in the cluster increases: a cluster formed by (H₂O)₁ - (CO)₂ absorbs at 2148.8 cm⁻¹, consistent with the peak position in the (3:2) ice of the current experiment. Experiments with deuterated water have shown that the CO - D₂O cluster produces an infrared absorption at 2150.2 cm⁻¹ (Abe & Yamada 2001). From these experiments, it can be concluded that when the cluster has only one CO molecule the band shifts toward the blue when the number of the H₂O molecules increases in the cluster.

Thus, given the positions and the FWHM of the band at about 2150 cm⁻¹ in the current experiment, it is possible to describe the ice structure before irradiation as a collection of (H₂O)_m - (CO)_n clusters with the cluster most abundant in the ice depending on the ice concentration. Clearly, in the (3:2) concentration, the (H₂O)₁ - (CO)₂ cluster is the most abundant while in the (10:1) concentration the most abundant is the (H₂O)_m - (CO)₁ cluster with $m > 1$.

The 2150 cm⁻¹ component is rapidly destroyed by irradiation in the (3:2) ice concentration. The component vanishes after an irradiation fluence of 5×10^{11} ions.cm⁻². Both the peak position and the FWHM do not vary with the irradiation. At (10:1) concentration, the component persists until an irradiation fluence of 2.5×10^{12} ions.cm⁻². The position shifts toward the red component to 2150.7 cm⁻¹ and the band narrows to 5.9 cm⁻¹. These results suggest that the OH dangling groups form bonds with other molecules decreasing the number of sites available to interact with CO. Furthermore, the redshift and the narrowing of the band in the (10:1) concentration suggest that the ice morphology changes,

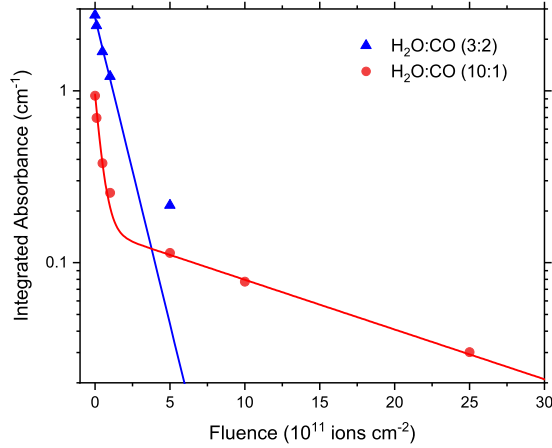


Figure 7. 2150 cm^{-1} component integrated absorbance as a function of fluence. For the (3:2) ice, data are fitted by only one exponential function while the (10:1), they are fitted by the sum of two exponential functions.

as the hydrogen bonds are formed: the number of the big clusters decreases leaving the ice with a distribution of smaller clusters before the disappearance of the band.

Figure 7 shows the 2150 cm^{-1} integrated absorbance as a function of fluence for both concentrations. In the (3:2) concentration, the 2150 cm^{-1} integrated absorbance decreases rapidly and can be fitted by only one exponential function. For the (10:1) concentration, the decrease of integrated absorbance deviates from the only one exponential function and a second exponential summed to the first has to be used. The reason for distinct behavior between the two concentration experiments may lay on the difference in the ice thickness. The (3:2) ice thickness is 34% smaller than the (10:1) ice. Furthermore, the CO abundance in the (3:2) ice is higher than in the (10:1) ice which leaves the CO molecules exposed to desorption processes such as the sputtering. Indeed, the last value in the (3:2) ice starts to deviate to the one exponential function, showing that, besides the concentration, the ice thickness may play a role in the time of disappearance of this feature. A time scale for the disappearance of this feature in the ISM is computed and discussed in the next section.

Oddly, for the (3:2) concentration ice, the 2148.8 cm^{-1} band reappears on the infrared spectrum of the ice irradiated by 5.3×10^{13} ions. cm^{-2} . A possible explanation is that the CO molecules are diffusing into the pores of a water layer that was deposited on top of the ice due to the condensation of the residual gas. This hypothesis is supported by the presence of an infrared feature at about 3634 cm^{-1} associated with the OH dangling bonds along all of irradiation time. In other circumstances, this band vanishes at the beginning of the irradiation (Dartois et al. 2013).

The 2144 cm^{-1} component:

The 2144 cm^{-1} feature is a minor component in the CO vibration mode. Before irradiation, it is centered on 2144.4 cm^{-1} for the (3:2) ice and 2144.2 cm^{-1} for the (10:1) ice. A tentative assignment for this component is based on the collection of clusters picture used to describe the 2150 cm^{-1} feature above. (Abe & Yamada 2004) have found weak and broader peaks at 2148.1 and 2147.7 cm^{-1} that were tentatively assigned to $(\text{H}_2\text{O})_1 - (\text{CO})_3$ and $(\text{H}_2\text{O})_1 - (\text{CO})_4$, respectively. In other words, as the number of CO molecules in the clusters increases, the component position shifts toward the red component, the 2144 cm^{-1} component is due to the absorption of $(\text{H}_2\text{O})_1 - (\text{CO})_n$ clusters with $n > 4$. Furthermore, its integrated absorbance is 40% higher in the (3:2) ice supporting this assignment.

However, its behavior with the irradiation is very complex and difficult to interpret using the collection of clusters scenario. In the (3:2) concentration and in the fluence range of 0 - 1×10^{13} ions. cm^{-2} , the integrated absorbance oscillates between 0.23 and 0.12 cm^{-1} with an average of 0.17 cm^{-1} and a standard deviation of 0.04 cm^{-1} . Since the mean uncertainty of the integrated absorbance is 0.01 cm^{-1} , this variation is not caused by statistical uncertainties in the fitting and may be caused by other effects. After a fluence of 1×10^{13} ions. cm^{-2} , the component collapses along with the other components due to the effect of sputtering on the ice.

The same behavior happens for the (10:1) concentration: the mean integrated absorbance is 0.15 cm^{-1} with a standard deviation of 0.05 cm^{-1} against a statistical uncertainty of 0.003 cm^{-1} . If the 2144 cm^{-1} component is produced by larger clusters involving many CO molecules, it would be expected a similar behavior observed for the 2150 cm^{-1} component: a rapidly decrease in its integrated absorbance followed by its disappearance. However, it was observed a decrease in the integrated absorbance at the beginning of irradiation, specially in the (10:1) ice, followed by an increase at 1×10^{12} ions. cm^{-2} .

Pontoppidan et al. (2003) have observed a component at about 2143 cm^{-1} in the ISM which was tentatively assigned to the CO stretching vibration in a pure ice with a crystalline structure under polarized light from the source. Boogert et al. (2002) claimed that this band is due to CO interacting with another molecule in the ice. It should be noted that the 2144 cm^{-1} component is the most susceptible to systematic effects

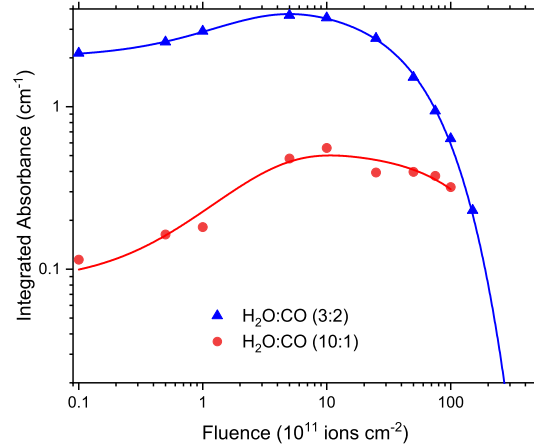


Figure 8. 2141 cm⁻¹ component integrated absorbance as a function of fluence. Data are fitted by Eq. 1.

produced by the decomposition process due to the presence of nearby strong components such as 2150 and 2141 cm⁻¹. Thus, it is not possible from the results of the current work to firmly assign this component to a specifically CO binding site.

The 2141 cm⁻¹ component:

The 2141 cm⁻¹ component could also be attributed to (H₂O)₁ - (CO)_n clusters with n > 4. However, when the number of CO molecules in the cluster increases, the interactions between them start to be important. (Abe & Yamada 2004) have assigned a peak at 2140.1 cm⁻¹ to CO - CO interactions (or CO dimer). Before irradiation, the positions of this component are 2140.8 cm⁻¹ (3:2) and 2141.2 cm⁻¹ (10:1). The proximity to the CO dimer at 2140.1 cm⁻¹ suggests that the 2141 cm⁻¹ component could be assigned to the CO dimer. The integrated absorbance is about 22 times greater for the (3:2) ice than for the (10:1) ice giving support to the CO dimer assignment.

The integrated absorbance of this component increases with irradiation for both ice concentrations (Figure 8, blue triangles). Its behavior is very similar to a daughter molecule integrated absorbance formed by radiolysis: it reaches a maximum at some fluence value (in the current experiment, 5 × 10¹¹ ions.cm⁻² for the (3:2) ice and 1 × 10¹² ions.cm⁻² for the (10:1) ice) followed by a decrease due to the ice desorption. The behavior of this component may be explained by the change of the CO binding site rather than to radiolysis. If the ices are a collection of (H₂O)_m - (CO)_n clusters, the changes in the m and/or n numbers of molecules would change the component in which the molecule will contribute. Furthermore, the participation of the OH dangling groups in the interactions with CO in the cluster also determines the infrared wavenumber in which the CO molecule absorbs. For example, as discussed above, the irradiation induces the OH dangling groups to form bonds with the water neighboring molecules causing the disappearance of the 2150 cm⁻¹ component. For the (3:2) ice, among the clusters with OH dangling interactions, the (H₂O)₁ - (CO)₂ cluster is the most abundant in the ice before irradiation starts. With the hydrogen bond formation, the interaction with an OH dangling group no longer exist and the interaction between the two remaining CO molecules could explain the increase in the 2141 cm⁻¹ component.

For the (10:1) ice, the clusters most abundant are those in which only one CO molecule interacts with many water molecules. Thus, a smaller number of CO dimers are produced by the irradiation induced hydrogen bonds. The comparison between the compaction cross sections (σ₁) gives evidence to support this interpretation: the decrease rate of the 2150 cm⁻¹ component for the (10:1) ice is 4.6 faster than for the (3:2) ice; however the 2141 cm⁻¹ component increases slowly for the (10:1) ice.

The 2138 cm⁻¹ component:

The 2138 cm⁻¹ component is one of the main components of the CO stretching vibration. (Abe & Yamada 2004) have assigned a peak at 2138.5 cm⁻¹ to the CO monomer vibration in librating sites. (Al-Halabi et al. 2004) attributes this component to substitutional CO replacing a water molecule in the matrix. However, pure CO ices also present a strong absorption peak at 2138.5 cm⁻¹.

In the current (3:2) ice experiment, this component is centered on 2138.6 cm⁻¹, consistent with the CO monomer position assigned by (Abe & Yamada 2004). For the (10:1) concentration, in which the absolute CO abundance is smaller, this component shifts toward the blue, at 2138.9 cm⁻¹, and presents a smaller integrated absorbance. The integrated absorbance ratio between the 2138 cm⁻¹ component and the total CO stretching vibration band is about 20% independently of the ice concentration (Al-Halabi et al. 2004).

The component behavior with the irradiation is totally dependent on the ice concentration. For the (3:2) concentration, the 2138 cm⁻¹ integrated absorbance variation is very similar to the 2141 cm⁻¹: it increases at the beginning of irradiation, reaches a maximum value at fluence of 5 × 10¹¹ ions cm⁻² (becomes one of the main component of the CO stretching vibration band) and decreases as the fluence continue to increase. If this component is generated by CO monomers in librating sites, its initial increase with irradiation shows that the collapse of the pores isolates the CO molecules in a new binding site. Indeed, in the (3:2) concentration, the number of clusters with two CO molecules is

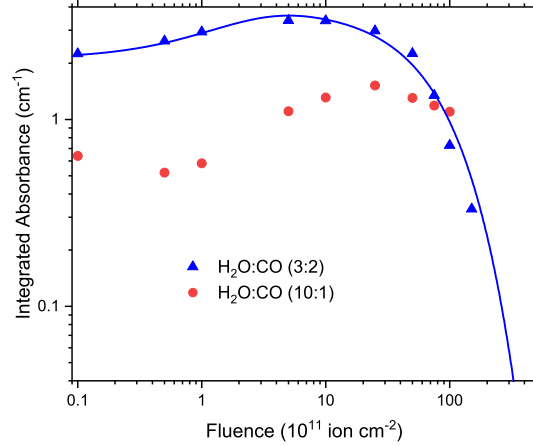


Figure 9. 2138 cm^{-1} component integrated absorbances as a function of fluence. The (3:2) data are fitted by Eq. 1.

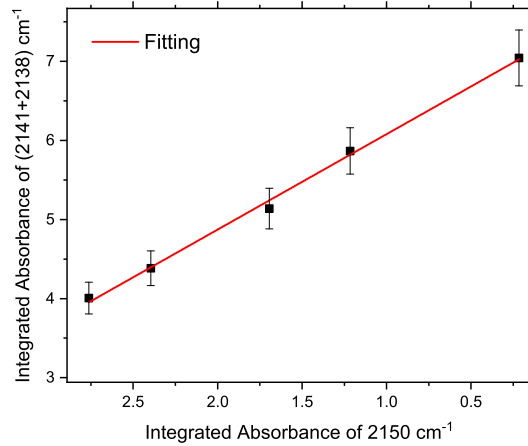


Figure 10. $2141 + 2138\text{ cm}^{-1}$ component integrated absorbance as a function of 2150 cm^{-1} integrated absorbance in the range $0 - 5 \times 10^{11}$ ions cm^{-2} . The x axis was inverted to show that when the 2150 cm^{-1} decreases as the sum of the 2141 and 2138 cm^{-1} increases. The data were fitted by a linear function with an angular coefficient of 1.2.

the most abundant in the ice, which contributes to the increase of the 2141 cm^{-1} component as discussed above. Nevertheless, given a FWHM of 10 cm^{-1} of the 2150 cm^{-1} component, the $(\text{H}_2\text{O})_m - (\text{CO})_1$ clusters with $m \geq 1$ are also abundant in the ice.

If the decrease of 2150 cm^{-1} is the main source for the CO monomers and dimers it should be expected an anti correlation between their integrated absorbances with an angular coefficient smaller than or equal to 1. Figure 10 shows the total integrated absorbance of 2141 and 2138 cm^{-1} components against the 2150 cm^{-1} component in the fluence range in which the ice structure is changing, i.e. from $0 - 5 \times 10^{11}$ ions cm^{-2} . The solid line represents a linear fit with a rate of 1.2 suggesting that the increase of these components, especially that presented by the 2138 cm^{-1} component, can not be fully explained by the destruction of the $(\text{H}_2\text{O})_m - (\text{CO})_1$ clusters. Other CO binding sites, such as those generating the 2136 cm^{-1} component as described below, may be contributing to increase the number of CO monomers.

For the (10:1) ice, the evolution of the 2138 cm^{-1} integrated absorbance is completely different from that presented in the (3:2) ice. Initially, the component decreases about 30%, a totally unexpected behavior given what is observed in the (3:2) ice and the fact that the population of clusters with only one CO molecule is the highest for the (10:1) concentration. The destruction of such clusters should increase the number of CO monomers in the ice. Indeed, the component increases after a fluence value of 5×10^{10} ions cm^{-2} and becomes the main component of the CO stretching vibration band at the end of the compaction process, after a fluence value of 5×10^{11} ions cm^{-2} .

This delay on the increase of 2138 cm^{-1} is a problem for the component assignment. Besides that, its shifted position toward the blue on the spectrum suggests that this component may have been influenced by other binding sites. (Al-Halabi et al. 2004) have assigned the 2139 cm^{-1} feature to a CO interface interaction with the hydrogen bonds. The formation of hydrogen bonds between the water molecules in the clusters

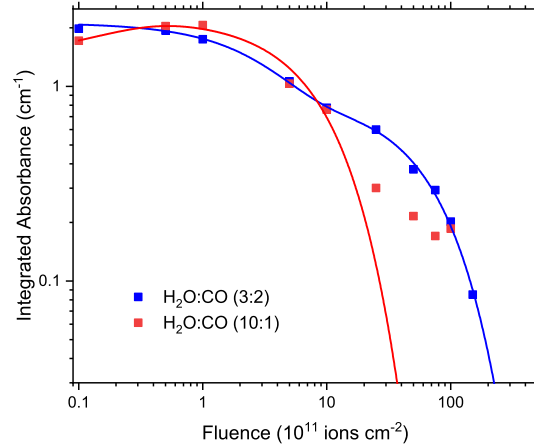


Figure 11. 2136 cm⁻¹ component integrated absorbance as a function of fluence. Data are fitted by Eq. 1.

by the irradiation produces many of these interactions with the CO molecules. Thus, even if the 2138 cm⁻¹ component has been influenced by this interaction, it should increase as the irradiation starts. The behavior of the 2136 cm⁻¹ component with irradiation may help to interpret the 2138 cm⁻¹ behavior.

The 2136 cm⁻¹ component:

Abe & Yamada (2004) assigned the 2136.7 cm⁻¹ component to the CO monomer in the nonlibrating sites. In the current work, the component is centered on 2136 cm⁻¹ for both ice concentrations. As the irradiation starts, the component behavior depends on the ice concentration. For the (3:2) ice, the integrated absorbance decreases as a function of fluence (Figure 11). If this component is produced by CO monomer vibrations, it is tentative to consider it as one of the sources for the increase of the 2138 cm⁻¹ component. In this case, only a change in the libration condition of the site would be necessary to change the vibration frequency of the molecule.

(Al-Halabi et al. 2004) claim that the 2136 cm⁻¹ evolves irreversibly from 2138 cm⁻¹ component when a mixed ice is warmed. However, in the current work, the opposite effect is observed: during the irradiation induced compaction process, the 2138 cm⁻¹ component increases as the 2136 cm⁻¹ component decreases. This is particularly remarkable in the (10:1) ice in which both components change with a phase difference of 180° (Figure 12).

The comparison between these two main components shows some interesting features: before irradiation, the 2136/total CO integrated absorbance ratio is dependent on the ice concentration: 22% for the (3:2) ice and 35% for the (10:1) ice. However, after an irradiation fluence of 1×10^{13} ions cm⁻², both converge to about 10%. Initially, the 2138/total ratio is about 20% and independent on the ice concentration; it increases for both concentrations by irradiation, although the maxima reached by them are different: 50% in the (3:2) ice (at 5×10^{12} ions.cm⁻²) and 60% in the (10:1) ice. As discussed above, at the end of irradiation the sputtering becomes important for the (3:2) ice due to its smaller thickness, making difficult for this component to reach greater relative abundances.

Thus, for both experiments concentration, the effect of irradiation in the CO monomers binding sites is to transform the nonlibrating sites into librating sites given the increase of the 2138 cm⁻¹ component. Furthermore, the change of the ice structure, with the formation of hydrogen bonds and the consequently collapse of the pores, make the CO molecules, interacting with the OH dangling bonds in the water clusters, be trapped in the ice matrix occupying sites in the lattice in the librating sites (preferentially) and nonlibrating sites. In view of the different ice concentrations studied here and given that the decrease of the ice thickness is different in each concentration (the ice thickness reduces 55% in the (3:2) concentration and 30% in the (10:1) concentration at fluence value of 1×10^{13} ions.cm⁻²), it is surprisingly that the final relative abundances of CO are approximately the same (~ 55% for the 2138 cm⁻¹ and ~ 10% for the 2136 cm⁻¹ component).

The 2133 cm⁻¹ component:

In the current work it is not possible to assign the 2133 cm⁻¹ component. There is no assignment found in the literature and its behavior with irradiation follows the 2136 cm⁻¹ component. Its integrated absorbance and FWHM are not negligible to consider it as a false component. It seems a CO binding site related to the CO monomer. However, more laboratory experiments need to be performed to assign this component.

3.3 The total CO stretching vibration integrated absorbance

Figure 13 shows the total CO column density as a function of fluence obtained from the sum of the all of integrated absorbance components and using the band strength of 1.1×10^{-17} cm molecule⁻¹ (Gerakines et al. 2005). The data are fitted by the sum of two exponential functions as shown in Eq. 1. It is clear that the decrease rate of the total CO column density in the (3:2) ice is higher than in the (10:1) ice. The ice

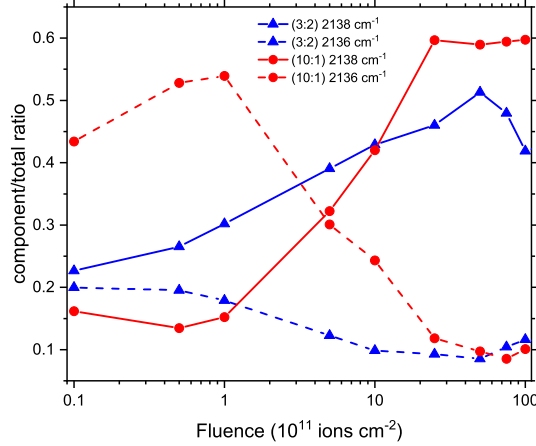


Figure 12. The ratio between the component integrated absorbance and the total CO integrated absorbance of the components 2138 and 2136 cm^{-1} .

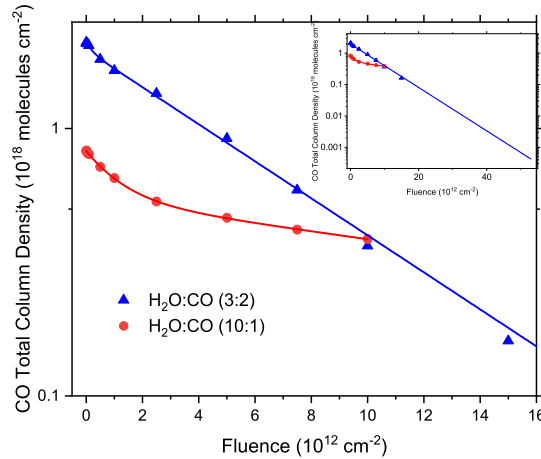


Figure 13. Total CO column density as a function of fluence. The column densities are obtained by summing the components integrated absorbance up and assuming an A-value = $1.1 \times 10^{-17} \text{ cm molecule}^{-1}$. The data are fitted by the sum of two exponential functions (solid lines; see Eq.(1)). The inset graph shows the total fluence range.

thickness difference between the two experiments may explain this result. The sputtering becomes relatively important in the (3:2) ice due to the smaller thickness of the (3:2) ice.

Furthermore, the formation of the hydrogen bonds and the migration of the CO molecules to the lattice binding sites make them more resistant to the irradiation effects. The cross sections obtained for the (3:2) ice is approximately 4.5 times greater than for the (10:1).

4 ASTROPHYSICAL IMPLICATIONS

The results of the decomposition presented here have implications to the understanding of the ISM ice structure. The laboratory spectra of mixed $\text{H}_2\text{O} + \text{CO}$ ices irradiated by swift heavy ions show a complex dynamic between the components of the CO stretching vibration profile as a function of the irradiation fluence. The CO band can be decomposed into six Gaussians functions and their changes with fluence could be monitored. Here, these components are described in view of the interactions of CO and water clusters.

In the ISM, the CO stretching vibration profile can be decomposed into only three components: 2143 cm^{-1} , 2139 cm^{-1} and 2136 cm^{-1} (Pontoppidan et al. 2003). The observations suggest a layered structure of the ices with a CO layer on top of water ice. This model is supported by the presence of a strong absorption at 2139 cm^{-1} . Furthermore, the observation of an anti-correlation between the 2139 cm^{-1} and 2136 cm^{-1} features suggests an evolutionary scenario for the mantle ices: in the quiescent regions the 2139 cm^{-1} feature relative to the 2136 cm^{-1} is higher. As the cloud evolves and star formation starts, the 2136 cm^{-1} becomes stronger and the 2139 cm^{-1} weakens such as observed in the

Table 5. Destruction cross sections (in 10⁻¹² cm²) of the absorption components due to distinct interactions: OH dangling bond vibration mode (OH db), CO and OH db (2150 cm⁻¹), the CO dimer vibration (2141 cm⁻¹), the CO monomer (2138 cm⁻¹) and CO and H₂O molecule in the bulk (2136 cm⁻¹).

Bands cm ⁻¹	(3:2)				(10:1)			
	σ_1	σ_2	S ₁ cm ⁻¹	S ₂ cm ⁻¹	σ_1	σ_2	S ₁ cm ⁻¹	S ₂ cm ⁻¹
2150	8.2	-	2.7	-	38	1.5	0.64	0.28
2141	5.6	0.20	-2.3	4.3	3.9	0.055	-0.46	0.54
2138	6.1	0.14	-1.8	4.0	-	-	-	-
2136	3.2	0.15	1.3	0.86	56	1.2	-0.83	2.2

line of sights towards YSOs. The interpretation for this observation is that, as the CO ice is being processed, the molecules on the surface evaporate (weakens the 2139 cm⁻¹ feature) and those on water interface migrate into the water matrix (strengthening the 2136 cm⁻¹ feature). This interpretation would imply that the ice should be porous in some degree for the CO molecules are trapped as the pore collapses with the processing of the ice. However, the component around 2150 cm⁻¹ is not found in the ISM, suggesting that the OH dangling site is no longer available to interact with the CO molecules.

The laboratory experiments have shown that such infrared feature is rapidly destroyed by thermal and energetic processing of the ice. In the current work, this component vanishes after fluence values of 5×10^{11} ions.cm⁻² (3:2) and 2.5×10^{12} ions.cm⁻² (10:1). The 2150 cm⁻¹ cross section measurements can be used to estimate the time scale (τ) of its disappearance in the ISM. The computation method is the same described by [Dartois et al. \(2013\)](#) in estimating the time scale for the loss of the dangling OH in a water ice,

$$\tau^{-1} = 4\pi \sum_Z \int_{E_{min}}^{\infty} \sigma_{2150}(E, Z) \frac{dN}{dE}(E, Z) dE \quad (2)$$

where σ_{2150} is the 2150 cm⁻¹ destruction cross section (Figure 6) and dN/dE is the cosmic ray differential flux ([Shen et al. 2004](#)). A potential law $\sigma(E) = R S_e(E)^n$, with $n = 1$, established experimentally by [Dartois et al. \(2013\)](#) was adopted for σ_{2150} . The proportionality constant R was evaluated by $R(0.79 \text{ MeV/u}) = \sigma_{2150}/S_e$ with the σ_{2150} obtained in the current work and considering that it is not dependent on Z . The electronic stopping power S_e was calculated using the SRIM code ([Ziegler et al. 2010](#)) as a function of energy and atomic number Z . Finally, the cross section $\sigma_{2150}(E, Z)$ was computed applying the potential law on the electronic stopping power $S_e(E, Z)$.

The functional form for the differential flux is given by [Webber & Yushak \(1983\)](#); [Shen et al. \(2004\)](#)

$$\frac{dN}{dE}(E, Z) = \frac{C E_0^{0.3}}{(E + E_0)^3} \quad (3)$$

where C is a normalization constant and E_0 is a parameter to adjust the low energy cosmic ray spectra. In the current work, $C = 9.42 \times 10^4$ ([Shen et al. 2004](#)) and $E_0 = 400 \text{ MeV}$ were used. The galactic cosmic rays (GCR) abundance adopted in this work was from [Meyer et al. \(1998\)](#) and the atomic species used in the time scale calculation were H, He, C, O, Mg, Si, Fe and Ni.

Thus, in the case of H₂O:CO ice concentration of (3:2), the time scale for the decrease of 2150 cm⁻¹ feature in ISM ice mantles would be about 1.4×10^6 years. In the case of an (10:1) ice concentration and considering each destruction regime separately, the time scales evaluated are 3×10^5 and 7.6×10^6 years, respectively. The first regime decreases the 2150 cm⁻¹ band to approximately 10 % to its initial value. Thus, considering that the destruction process in the first regime dominates 90% of the time and that the process in the second regime dominates the last 10% of the time, the total time scale for the disappearance of the 2150 cm⁻¹ feature in a (10:1) ice concentration in the ISM mantles is approximately 1×10^6 years.

These results are in agreement with the laboratory constraints for the loss of OH dangling bonds time scales [Dartois et al. \(2013\)](#) and with the observational constraints in which the 2150 cm⁻¹ feature is not observed in the ISM. Furthermore, if the ice mantles on the interstellar grains are formed by simultaneous accretion of H₂O and CO from the gas, the ice morphology change driven by cosmic ray particles occurs in 1 Ma time scale. Given the component changes observed here, at the end of this phase, the CO stretching vibration profile is dominated by the a combination of the 2141.1 and 2138.7 cm⁻¹ components.

The irradiation fluence range reached in the current work can be considered as the first million years of the ice mantles in the ISM, before the onset of the stellar formation. A sketch of the ice evolution can be drawn in this cloud stage. The ices studied here can be applied to the hypothesis in which the mantle ices are formed either by the chemical reactions on the surface of hydrogen and oxygen atoms concomitantly with the condensation of CO molecules from the gas or by the accretion of both molecules from the interstellar gas at the same time. Once the first monolayers of ice are formed, it is subjected to cosmic ray bombardment. The result of this irradiation is to produce an ice with a polycrystalline structure without pores and with substitutional CO molecules in the ice matrix. It generates a 2136 cm⁻¹ component with a 10% abundance relative to the CO stretching vibration band independent on the ice concentration. This is consistent with the observation that the 2136 cm⁻¹ component is always present in the ISM with a minimum abundance of 16% relative to the total CO molecule trapped in the ice ([Pontoppidan et al. 2003](#)).

Furthermore, if the 2141 cm^{-1} component is attributed to the CO dimers absorptions it could be associated to the ISM 2139 cm^{-1} component. Note that the 2141 cm^{-1} component also increases with irradiation becoming one of the main components of the CO stretching band (together with the 2138 cm^{-1} component). This is especially true in the (3:2) ice concentration in which the abundance of CO is higher. The CO stretching vibration band of a $\text{H}_2\text{O}:\text{CO}$ ice mixture irradiated by heavy ions is equivalent to those of ISM in direction of quiescent regions in which the 2139 cm^{-1} component is the main component and the 2136 cm^{-1} is about 16% of the band. In other words, what would be observed by the surveys is the ice mantles processed by irradiation at the end of the first stage of the cloud evolution in which the ices are formed.

An important problem related to the absorbance increase of the 2138 cm^{-1} component. Why this component is not observed in the ISM? Could it be an evidence that the cosmic rays distribution flux is smaller than that used here? A smaller cosmic rays flux would increase the time scale for the disappearance of the 2150 cm^{-1} component which would increase the probability to detect it in the ISM. Another possibility is that the CO binding sites in the ISM ice mantles are constituted by only non librating sites since that only the 2136 cm^{-1} component is detected.

5 CONCLUSIONS

The aim of the current work is to analyze the molecular rearrangements occurring when a $\text{H}_2\text{O} + \text{CO}$ mixture is irradiated. These processes, known under a general name of compaction, are different from the ice radiolysis. They correspond to transitions triggered when part of the energy transferred by the projectile allows atoms or molecules over passing potential barriers and ending up in stronger chemical bonds (links), i.e., minimizing the total potential energy of the system. We identified several rearrangements; all of them occur at the beginning of the irradiation and last different time intervals to reach the steady state.

The CO stretching vibration band is decomposed into six components: 2150, 2144, 2141, 2138, 2136 and 2133 cm^{-1} . In the current work, the cluster scenario is used to describe the sites in which the CO components were assigned. The cross sections for the evolution of the main component are obtained by fitting their evolution as a function of projectile fluence using two exponential functions.

Based on the results obtained, the time scale for the disappearance of the 2150 cm^{-1} component induced by cosmic rays species is computed. After a time scale of 1 Ma, the ice pores collapse vanishes the 2150 cm^{-1} component and rearranges the CO binding sites. The 2136 cm^{-1} component, attributed to the substitutional CO in a water matrix in non-librating sites started as the main component of the ice due to the co-deposition of the molecules. However, the 2138 cm^{-1} and 2141 cm^{-1} components become the main components of the CO stretching vibration band. The 2144 cm^{-1} component, is tentatively attributed in this work to a cluster such as $(\text{CO})_m - (\text{H}_2\text{O})_1$, with $m > 4$, is a minor component of the ice after 1 Myrs. It was not possible to assign the 2133 cm^{-1} component. However, this behavior is correlate with the 2136 cm^{-1} component suggesting a relation with the CO monomer sites.

We propose that the abundance of the CO monomers in the dust grain ices increase under irradiation, even if the initial CO concentration is low. The relative abundances between components can indeed be used as a time indicator of the chemical evolution of the ice.

ACKNOWLEDGMENTS

The French-Brazilian exchange program CAPES-COFECUB, as well as the CNPq (INEspaço), Bolsa de Produtividade - CNPq (301868/2017-4), Projeto Universal - CNPq (407938/2018-4), FINEP (0647/18), Cientista do Nosso Estado - FAPERJ (E-26/202.549/2019 and E-26/202.843/2018) and FAPERJ (E-26/203.204/2017, E-26/241.202/18 and E-26/45.307/19) are acknowledged for partial support. This study was financed in part by the Coordenação de Aperfeiçoamento de Pessoal de Nível Superior - Brazil (CAPES) - Finance Code 001. We are grateful to T. Been, C. Grygiel and J. M. Ramillon for their invaluable assistance during the experiments.

6 DATA AVAILABILITY

The data underlying this article will be shared on reasonable request to the corresponding author.

REFERENCES

- Abe, H., Takeo, H., & Yamada, K. M., 1999, *Chemical physics letters*, 311(3-4), 153-158.
 Abe, H., & Yamada, K. M., 2001, *JPC*, 114(14), 6134-6141.
 Abe, H., & Yamada, K. M., 2003, *Structural Chemistry*, 14(2), 211-215.
 Abe, H., & Yamada, K. M., 2004, *JPC*, 121(16), 7803-7812.
 Aikawa, Y., Ohashi, N., Inutsuka, S. I., Herbst, E., & Takakuwa, S., 2001, *APJ*, 552(2), 639.
 Al-Halabi, A., Fraser, H. J., Kroes, G. J., & Van Dishoeck, E. F., 2004, *A&A*, 422(3), 777-791.
 Andrade, D. P., de Barros, A. L., Pilling, S., Domaracka, A., Rothard, H., Boduch, P., & da Silveira, E. F., 2013, *MNRAS*, 430(2), 787-796.
 Bennett, C. J., Jamieson, C. S., Osamura, Y., & Kaiser, R. I., 2005, *APJ*, 624(2), 1097.
 Bennett, Chris J., & Ralf I. Kaiser, 2007, *APJ* 661.2, 899.
 Bernstein, M. P., Sandford, S. A., & Allamandola, L. J., 1996, *APJ Letters*, 472(2), L127.

- Bernstein, M. P., Cruikshank, D. P., & Sandford, S. A., 2005, *Icarus*, 179(2), 527-534.
- Boduch, P., Domaracka, A., Fulvio, D., Langlinay, T., Lv, X. Y., Palumbo, M. E., ... & Strazzulla, G., 2012, *A&A*, 544, A30.
- Boogert, A. C., & Ehrenfreund, P., 2004, In *Astrophysics of Dust* (Vol. 309, p. 547).
- Boogert, A. C. A., Blake, G. A., & Tielens, A. G. G. M., 2002, *APJ*, 577(1), 271.
- Bouilloud, M., Fray, N., Bénilan, Y., Cottin, H., Gazeau, M. C., & Jolly, A., 2015, *MNRAS*, 451(2), 2145-2160.
- Bouwman, J., Henning, T., Hillenbrand, L. A., Meyer, M. R., Pascucci, I., Carpenter, J., ... & Wolf, S., 2008, *APJ*, 683(1), 479.
- Bouwman, J., Ludwig, W., Awad, Z., Öberg, K. I., Fuchs, G. W., van Dishoeck, E. F., & Linnartz, H., 2007, *A&A*, 476(2), 995-1003.
- Chiar, J. E., Adamson, A. J., Kerr, T. H., & Whittet, D. C. B., 1994, *APJ*, 426, 240-248.
- Collings, M. P., Dever, J. W., Fraser, H. J., McCoustra, M. R. S., & Williams, D. A., 2003, *APJ*, 583(2), 1058.
- Dartois, E., Ding, J. J., De Barros, A. L. F., Boduch, P., Brunetto, R., Chabot, M., ... & Pino, T., 2013, *A&A*, 557, A97.
- Dartois, E., Augé, B., Boduch, P., Brunetto, R., Chabot, M., Domaracka, A., ... & Da Silveira, E. F., 2015, *A&A*, 576, A125.
- de Barros, A. L. F., Bordalo, V. S. D. E., Duarte, E. S., da Silveira, E. F., Domaracka, A., Rothard, H., & Boduch, P., 2011, *A&A*, 531, A160.
- de Barros, A. L. F., Domaracka, A., Andrade, D. P. P., Boduch, P., Rothard, H., & da Silveira, E. F., 2011b, *MNRAS*, 418(2), 1363-1374.
- de Barros, A. L. F., Boduch, P., Domaracka, A., Rothard, H., & da Silveira, E. F., 2012, *Low Temperature Physics/Fizika Nizkikh Temperatur*, 38(8), 953-960.
- de Barros, A. L. F., da Silveira, E. F., Rothard, H., Langlinay, T., & Boduch, P., 2014, *MNRAS*, 443(3), 2733-2745.
- de Barros, A. L. F., da Silveira, E. F., Bergantini, A., Rothard, H., & Boduch, P., 2015, *APJ*, 810(2), 156.
- de Barros, A. L. F., da Silveira, E. F., Fulvio, D., Rothard, H., & Boduch, P., 2016, *APJ*, 824(2), 81.
- de Barros, A. L. F., da Silveira, E. F., Fulvio, D., Boduch, P., & Rothard, H., 2016, *MNRAS*, 465(3), 3281-3290.
- Duarte, E. S., Domaracka, A., Boduch, P., Rothard, H., Dartois, E., & Da Silveira, E. F., 2010, *A&A*, 512, A71.
- Duarte, E. S., Boduch, P., Rothard, H., Been, T., Dartois, E., Farenzena, L. S., & Da Silveira, E. F., 2009, *A&A*, 502(2), 599-603.
- Eiroa, C., & Hodapp, K. W. (1989). Ice dust grains in the Serpens molecular cloud. *A&A*, 210, 345-350.
- Elsila, J., Allamandola, L. J., & Sandford, S. A., 1997, *APJ*, 479(2), 818.
- Gerakines, P. A., Schutte, W. A., Greenberg, J. M., & van Dishoeck, E. F., 1994, arXiv preprint astro-ph/9409076.
- Gerakines, P. A., Schutte, W. A., & Ehrenfreund, P., 1996, *A&A*, 312, 289-305.
- Gerakines, P. A., Bray, J. J., Davis, A., & Richey, C. R., 2005, *APJ*, 620(2), 1140.
- Hagen, W., Tielens, A. G. G. M., & Greenberg, J. M., 1981, *Chemical Physics*, 56(3), 367-379.
- Hudson, R. L., & Moore, M. H., 1999, *Icarus*, 140(2), 451-461.
- Hudson, R. L., & Moore, M. H., 2000, *A&A*, 357, 787-792.
- Ioppolo, S., Cuppen, H. M., Romanzin, C., Van Dishoeck, E. F., & Linnartz, H., 2008, *APJ*, 686(2), 1474.
- Jamieson, C. S., Mebel, A. M., & Kaiser, R. I., 2006, *ApJS*, 163(1), 184.
- Kerr, T. H., Adamson, A. J., & Whittet, D. C. B., 1993, *MNRAS*, 262(4), 1047-1056.
- Loeffler, M. J., & Baragiola, R. A., 2005, *Geophysical research letters*, 32(17).
- Loeffler, M. J., Baratta, G. A., Palumbo, M. E., Strazzulla, G., & Baragiola, R. A., 2005a, *A&A*, 435(2), 587-594.
- Loeffler, M. J., Teolis, B. D., & Baragiola, R. A., 2006, *JPC*, 124(10), 104702.
- Loeffler, M. J., & Baragiola, R. A., 2010, *JCP*, 133(21), 214506.
- Mejía, C., de Barros, A. L. F., Bordalo, V., da Silveira, E. F., Boduch, P., Domaracka, A., & Rothard, H., 2013, *MNRAS*, 433(3), 2368-2379.
- Mejía C., de Barros, A. L. F., Duarte, E. S., da Silveira, E. F., Dartois, E., Domaracka, A., ... & Boduch, P., 2015, *Icarus*, 250, 222-229.
- Mejía, C., de Barros, A. L. F., Rothard, H., Boduch, P., & da Silveira, E. F., 2020, *APJ*, 894(2), 132.
- Meyer, J., O'C Drury, L., & Ellison, D. C. 1998, *Space Sci. Rev.*, 86, 179.
- Moore, M. H., & Hudson, R. L., 2000, *Icarus*, 145(1), 282-288.
- Palumbo, M. E., Castorina, A. C., & Strazzulla, G., 1999, *A&A*, 342, 551-562.
- Pereira, R. C., de Barros, A. L. F., da Costa, C. A. P., Oliveira, P. R. B., Fulvio, D., & da Silveira, E. F., 2020, *MNRAS*, 495(1), 40-57.
- Pontoppidan, K. M., Fraser, H. J., Dartois, E., Thi, W. F., Van Dishoeck, E. F., Boogert, A. C. A., ... & Bisschop, S. E., 2003, *A&A*, 408(3), 981-1007.
- Pontoppidan, K. M., 2006, *A&A*, 453(3), L47-L50.
- Rothard, H., Domaracka, A., Boduch, P., Palumbo, M. E., Strazzulla, G., Da Silveira, E. F., & Dartois, E., 2017, *J PHYS B-AT MOL OPT*, 50(6), 062001.
- Sandford, S. A., Allamandola, L. J., Tielens, A. G. G. M., & Valero, G. J., 1988, *APJ*, 329, 498-510.
- Schutte, W. A., Boogert, A. C. A., Tielens, A. G. G. M., Whittet, D. C. B., Gerakines, P. A., Chiar, J. E., ... & De Graauw, T. H., 1999, *A&A*, 343, 966-976.
- Schutte, W. A., Allamandola, L. J., & Sandford, S. A., 1993, *Icarus*, 104(1), 118-137.
- Shen, C. J., Greenberg, J. M., Schutte, W. A., & Van Dishoeck, E. F., 2004, *A&A*, 415(1), 203-215.
- Tielens, A. G. G. M., & Hagen, W., 1982, *A&A*, 114, 245-260.
- Tielens, A. G. G. M., Tokunaga, A. T., Geballe, T. R., & Baas, F., 1991, *APJ*, 381, 181-199.
- Trottier, A., & Brooks, R. L., 2004, *APJ*, 612(2), 1214.
- Watanabe, N., Nagaoka, A., Shiraki, T., & Kouchi, A., 2004, *APJ*, 616(1), 638.
- Watanabe, N., Mouri, O., Nagaoka, A., Chigai, T., Kouchi, A., & Pirronello, V., 2007, *APJ*, 668(2), 1001.
- Webber, W. R., & Yushak, S. M. 1983, *ApJ*, 275, 391.
- Xu-Yang Thesis (2013)
- Ziegler, James F., M. D. Ziegler, & J. P. Biersack, 2010, *NUCL INSTRUM METH B*, 268, no. 11, 1818-1823.